Flow harmonics v_n at finite density

Yoshitaka Hatta,[1] Akihiko Monnai,[2] and Bo-Wen Xiao[3]

[1]*Yukawa Institute for Theoretical Physics, Kyoto University, Kyoto 606-8502, Japan*
[2]*RIKEN BNL Research Center, Brookhaven National Laboratory, Upton 11973 New York, USA*
[3]*Key Laboratory of Quark and Lepton Physics (MOE) and Institute of Particle Physics,
Central China Normal University, Wuhan 430079, China*

We investigate the Gubser solution of viscous hydrodynamics at finite density and analytically compute the flow harmonics v_n. We explicitly show how v_n and their viscous corrections depend on the chemical potential. The difference in v_n between particles and antiparticles is also analytically computed and shown to be proportional to various chemical potentials and the viscosity. Excellent agreement is obtained between the results and the available experimental data from the SPS, RHIC and the LHC.

I. INTRODUCTION

Relativistic hydrodynamics is a general theoretical framework to describe the collective dynamics of high-energy systems near local thermal equilibrium. Its first application to hadron physics dates back to Landau's attempt to describe multiparticle production in hadron-hadron collisions [1]. It has become a topic of great interest since the discovery of the quark-gluon plasma (QGP) as a nearly perfect fluid in the "Little Bangs" at BNL Relativistic Heavy Ion Collider (RHIC) [2–5] and CERN Large Hadron collider (LHC) [6–8]. This is supported by the observations that the azimuthal momentum anisotropy of hadronic distribution [9,10], characterized by flow harmonics v_n, are found to reflect the geometrical anisotropy ϵ_n of the overlapping region of two colliding nuclei, and that they are in good quantitative agreement with theoretical estimations. Nowadays the viscous hydrodynamic modeling is considered as one of the most powerful tools to quantify the QGP medium near the crossover phase transition [11].

The recent beam energy scan (BES) experiments at RHIC pose us intriguing challenges to study the properties of the medium at finite density and to explore the QCD phase diagram to find signs of a critical point [12]. Conserved charges such as net baryon number, strangeness and isospin would play important roles in the collisions with lower energies, as the differences between particle and antiparticle yields are clearly seen [13,14]. Historically, it had long been speculated based on several idealized calculations that the strong coupling limit is achieved only at highest energies of RHIC experiments. On the other hand, recent improvements in off-equilibrium hydrodynamic modeling motivate us to reexamine the validity of hydrodynamics in exploring the dense quark matter created at midlow energies, especially since the differential elliptic flow $v_2(p_T)$ is found to remain large in phase I of the BES experiments. The applicability of hydrodynamic models is closely related to the origin of fluidity, about which little is known, and thus its verification would be a very important step towards a full understanding of the hot QCD medium.

So far many hydrodynamic analyses have been performed numerically because it is generally quite nontrivial to solve the partial differential equations involved. Analytical solutions of relativistic hydrodynamics, on the other hand, can be obtained with certain symmetry conditions and they are very instructive in understanding the essence of heavy-ion dynamics. The boost-invariant Bjorken flow [15] is one such classic example. More recently, Gubser found an exact boost-invariant solution of the Navier-Stokes equation which has a nontrivial dependence on the transverse coordinate [16]. The latter solution has the advantage that one can add azimuthally anisotropic perturbations [17,18] and analytically compute the corresponding flow harmonics v_n including the viscosity effects [18,19] (see, also, [20–22]).

In this study, we investigate v_n at finite density by analytically solving the viscous hydrodynamic equations coupled with conserved currents assuming conformal and boost-invariant symmetries. Aside from the fact that the solution itself is new and of theoretical importance, it gives us a theoretical guidance about the behavior of v_n over a wide range of the beam energy for which there are not many numerical simulations [23–27] and the previous knowledge obtained through the precision analyses in the RHIC-LHC energy regime, such as the value of the shear viscosity η/s, are no longer fully applicable. We discuss extensively the nature of flow in the presence of currents and estimate the beam energy (or chemical potential) dependence of v_n. The difference in v_n between particles and antiparticles is also analytically computed. The results are compared with the experimental data from SPS, RHIC and the LHC [13,14,28,29]. We see that they are in qualitative agreement, which suggests that a reasonable description of the low-energy

experimental data might be possible within a hydrodynamic framework.

The paper is organized as follows. The basic setup of relativistic hydrodynamics is outlined in Sec. II. We then present analytical formulas of the flow harmonics v_n in the ideal and viscous cases in Secs. III and IV, respectively. Phenomenological inputs for our model are summarized in Sec. V. Using these formulas and input parameters, we compare our results with the experimental data in Sec. VI. Section VII is devoted to summary and conclusions.

II. HYDRODYNAMIC EQUATIONS

A. Setup

We shall consider hydrodynamics of a conformal theory. The system is characterized by the local temperature T and a set of local chemical potentials μ_i where the subscript i labels various conserved charges of the theory. The flow velocity is denoted by u^μ with the normalization $u^\mu u_\mu = -1$. The energy-momentum tensor in the Navier-Stokes approximation takes the form

$$T^{\mu\nu} = \frac{4\varepsilon}{3} u^\mu u^\nu + \frac{\varepsilon}{3} g^{\mu\nu} - 2\eta\sigma^{\mu\nu}, \qquad (1)$$

where $\sigma^{\mu\nu}$ is the shear tensor and η is the shear viscosity. In (1), the conformal equation of state $\varepsilon = 3p$ between the energy density ε and the pressure p has been used. The conserved current J_i^μ associated with the chemical potential μ_i can be written as

$$J_i^\mu = n_i u^\mu - \kappa_i(u^\mu u^\nu + g^{\mu\nu})\partial_\nu\left(\frac{\mu_i}{T}\right), \qquad (2)$$

where n_i is the charge density and κ_i is the charge conductivity. The hydrodynamic equations consist of the conservation equations for $T^{\mu\nu}$ and J_i^μ,

$$\nabla_\mu T^{\mu\nu} = 0, \qquad \nabla_\mu J_i^\mu = 0, \qquad (3)$$

where ∇_μ is the covariant derivative.

Since there is no intrinsic mass scale in a conformal theory, the energy density ε and the charge densities n_i can be generically written as

$$\varepsilon = T^4 f\left(\frac{\mu_1}{T}, \frac{\mu_2}{T}, \ldots\right), \qquad n_i = \mu_i T^2 g_i\left(\frac{\mu_1}{T}, \frac{\mu_2}{T}, \ldots\right). \qquad (4)$$

With a view to applying to heavy-ion collisions, we shall focus on the following representative situation. We assume that there is the leading current $J^\mu = nu^\mu + \cdots$ ("baryon number current") and the corresponding chemical potential μ is treated to all orders. In addition, there is one subleading current $\tilde{J}^\mu = \tilde{n}u^\mu + \cdots$ ("isospin number current") whose chemical potential $\tilde{\mu}$ is small and treated only to linear

order. We take $\tilde{\mu}$ to be "orthogonal" to μ, in that $\varepsilon(\mu, \tilde{\mu})$ is invariant under a sign flip $\tilde{\mu} \leftrightarrow -\tilde{\mu}$ (i.e., cross terms like $\mu\tilde{\mu}T^2$ are absent). With these assumptions, we can parametrize

$$\varepsilon = T^4 f\left(\frac{\mu}{T}\right), \quad n = \mu T^2 g\left(\frac{\mu}{T}\right), \quad \tilde{n} = \tilde{\mu}T^2\tilde{g}\left(\frac{\mu}{T}\right). \qquad (5)$$

The last equation may be written as $\tilde{n} = \tilde{\mu}\tilde{\chi}$ where $\tilde{\chi} \propto \partial^2 p/\partial\tilde{\mu}^2|_{\tilde{\mu}=0}$ is the susceptibility.

B. Gubser flow

We shall solve the hydrodynamic equations (3) for a given flow velocity,

$$u^\tau = \cosh\left[\tanh^{-1}\frac{2\tau x_\perp}{L^2 + \tau^2 + x_\perp^2}\right],$$

$$u^\perp = \sinh\left[\tanh^{-1}\frac{2\tau x_\perp}{L^2 + \tau^2 + x_\perp^2}\right], \qquad (6)$$

and $u^\zeta = u^\phi = 0$. The parameter L is the characteristic length scale of the system. In heavy-ion collisions, it is roughly the transverse size of the colliding nuclei. Equation (6) is called Gubser flow [16,17] expressed in the coordinate system

$$ds^2 = -d\tau^2 + \tau^2 d\zeta^2 + dx_\perp^2 + x_\perp^2 d\phi^2, \qquad (7)$$

where $\tau = \sqrt{t^2 - x_3^2}$ is the proper time, $\zeta = \tanh^{-1}\frac{x_3}{t}$ is the spacetime rapidity and $x_\perp = \sqrt{x_1^2 + x_2^2}$ is the transverse coordinate. The condition $u^\zeta = 0$ means that the flow is boost invariant along the beam (x_3) direction.

Gubser flow takes a very simple form in a cleverly chosen coordinate system $\hat{x}^\mu$ which is related to the Minkowski coordinates via a Weyl rescaling of the metric:

$$d\hat{s}^2 = \frac{ds^2}{\tau^2} = -d\rho^2 + \cosh^2\rho(d\Theta^2 + \sin^2\Theta d\phi^2) + d\zeta^2, \qquad (8)$$

where

$$\sinh\rho = -\frac{L^2 - \tau^2 + x_\perp^2}{2L\tau}, \qquad \tan\Theta = \frac{2Lx_\perp}{L^2 + \tau^2 - x_\perp^2}. \qquad (9)$$

In this coordinate system, the flow velocity is simply $\hat{u}^\mu = \delta_\rho^\mu$. In addition to the boost invariance, the flow respects the $O(3)$ symmetry with respect to the "polar" angles (Θ, ϕ). Variables in this coordinate system will be denoted with a "hat," e.g., $\hat{u}^\mu$, $\hat{\varepsilon}$.

III. INVISCID CASE

In this section, we solve the hydrodynamic equations (3) in the ideal case $\eta = \kappa_i = 0$. We then deform the solution in the azimuthal direction ϕ and compute flow harmonics v_n.

A. Isotropic ideal solution

The isotropic solution (i.e., independent of ϕ) has been obtained already in [16,17] in the presence of a current $J^\mu = nu^\mu$. Assuming that all the quantities depend only on ρ, we can readily solve the hydrodynamic equations for $\hat{\varepsilon}_0$ and $\hat{n}_0$ in the coordinates (8). We then perform the Weyl transformation back to the Minkowski space $\varepsilon_0 = \hat{\varepsilon}_0/\tau^4$, $n_0 = \hat{n}_0/\tau^3$ to get

$$\varepsilon_0 = T_0^4 f\left(\frac{\mu_0}{T_0}\right) \propto \frac{1}{\tau^4 (\cosh\rho)^{8/3}}, \qquad (10)$$

$$n_0 = \mu_0 T_0^2 g\left(\frac{\mu_0}{T_0}\right) \propto \frac{1}{\tau^3 \cosh^2\rho},$$

$$\tilde{n}_0 = \tilde{\mu}_0 T_0^2 \tilde{g}\left(\frac{\mu_0}{T_0}\right) \propto \frac{1}{\tau^3 \cosh^2\rho}. \qquad (11)$$

These equations can be solved for T_0 and μ_0. It is consistent to look for the solution where T_0 and μ_0 have the same ρ-dependence such that the ratios $\alpha \equiv \mu_0/T_0$, $\tilde{\alpha} \equiv \tilde{\mu}_0/T_0$ are independent of ρ. We find

$$T_0 = \frac{C}{\tau(\cosh\rho)^{2/3}}, \quad \mu_0 = \frac{\alpha C}{\tau(\cosh\rho)^{2/3}}, \quad \tilde{\mu}_0 = \frac{\tilde{\alpha} C}{\tau(\cosh\rho)^{2/3}}, \qquad (12)$$

and therefore

$$\varepsilon_0 = \frac{f(\alpha)C^4}{\tau^4(\cosh\rho)^{8/3}}, \qquad n_0 = \frac{\alpha g(\alpha)C^3}{\tau^3 \cosh^2\rho}, \qquad \tilde{n}_0 = \frac{\tilde{\alpha}\tilde{g}(\alpha)C^3}{\tau^3 \cosh^2\rho}. \qquad (13)$$

The parameter C is related to the particle multiplicity to be extracted from the experimental data. For a massless particle species i ("pion"), the relation is [16,19]

$$\frac{dN_i}{dY} \approx g_i \frac{4C^3}{\pi}, \qquad (14)$$

where Y is the momentum rapidity and g_i is the degeneracy factor.

B. Anisotropic ideal solution

We now perturb the solution anisotropically to introduce the $\cos n\phi$ dependence. In doing so, we shall focus on the early time regime $\tau \ll L$ [or $\rho \to -\infty$, see (9)]. As observed in [19], in this regime the perturbed solution is

fully under analytical control including the viscous case to be discussed in the next section.

Following [17], we consider the following deformation of the isotropic solution:

$$\hat{\varepsilon}_0 \to \hat{\varepsilon} = \hat{\varepsilon}_0 (1 - \epsilon_n \mathcal{A}\delta)^4,$$

$$\hat{n}_0 \to \hat{n} = \hat{n}_0 (1 - \epsilon_n \mathcal{A}\delta')^3,$$

$$(\hat{u}^\rho, \hat{u}^\Theta, \hat{u}^\phi, \hat{u}^\zeta) = (1, 0, 0, 0)$$
$$\to (1, -\epsilon_n \nu_s \hat{g}^{\Theta\Theta} \partial_\Theta \mathcal{A}, -\epsilon_n \nu_s \hat{g}^{\phi\phi} \partial_\phi \mathcal{A}, 0), \qquad (15)$$

where

$$\mathcal{A} \equiv \left(\frac{2Lx_\perp}{L^2 + x_\perp^2}\right)^n \cos n\phi \qquad (16)$$

is proportional to the spherical harmonics $Y_{n,n}(\Theta, \phi) + Y_{n,-n}(\Theta, \phi)$ in the early time regime $\tau \ll L$. Note that we preserve boost invariance $u^\zeta = 0$ in this paper, but the case $u^\zeta \neq 0$ was also considered in [17]. ϵ_n is the eccentricity[1] which we assume to be small $\epsilon_n \ll 1$ and keep only linear terms in ϵ_n. $\delta(\rho)$, $\delta'(\rho)$ and $\nu_s(\rho)$ have to be determined by solving the hydrodynamic equations linearized around the isotropic solution. Plugging (15) into (3), we find the following equation for δ':

$$\partial_\rho \delta' = \frac{\nu_s}{3\cosh^2\rho} n(n+1). \qquad (18)$$

This turns out to be exactly the same as the equation satisfied by δ [17]. Therefore, in the ideal case we have $\delta = \delta'$, which means that T_0 and μ_0 are rescaled by the same factor $T = T_0(1 - \epsilon_n \mathcal{A}\delta)$, $\mu = \mu_0(1 - \epsilon_n \mathcal{A}\delta)$ and $\tilde{\mu} = \tilde{\mu}_0(1 - \epsilon_n \mathcal{A}\delta)$. The ratios $\mu/T = \mu_0/T_0 = \alpha$ and $\tilde{\mu}/T = \tilde{\mu}_0/T_0 = \tilde{\alpha}$ are thus unchanged. At early times $\rho \to -\infty$, the right-hand side of (18) is negligible and we can set $\delta = 1$ [19].

C. v_n at finite μ

In order to compute flow harmonics v_n, we use the Cooper-Frye formula [30]

---

[1]In a conformal theory, the definition of eccentricity requires some care. We use [17,19]

$$\epsilon_n = -\frac{\int d^2 x_\perp \varepsilon^{3/4} \frac{x_\perp^n}{(L^2 + x_\perp^2)^{n-1}} \cos n\phi}{\int d^2 x_\perp \varepsilon^{3/4} \frac{x_\perp^n}{(L^2 + x_\perp^2)^{n-1}}}. \qquad (17)$$

$$(2\pi)^3 \frac{dN_i}{dY p_T dp_T d\phi_p}$$

$$= g_i \int_\Sigma (-p^\mu d\sigma_\mu) \left(\exp\left(\frac{u \cdot p + k\mu_i}{T} \right) + \delta f \right)$$

$$\propto 1 + 2v_n(p_T) \cos n\phi_p, \qquad (19)$$

where we assumed the Boltzmann distribution and δf is the deviation from the equilibrium distribution. The use of the Boltzmann distribution (rather than the Fermi/Bose distributions) may be justified for the purpose of computing the integrated v_n [19]. μ_i generically represents a set of chemical potentials for net baryon number, isospin and strangeness. We assign $k = \pm 1$ for particles with positive/negative quantum numbers mentioned above, and $k = 0$ for neutral particles with respect to the corresponding quantum number. In principle, since we are assuming conformal symmetry, the formula (19) should be used only for massless particles, or particles that can be approximately treated as massless (i.e., pions). However, for the sake of discussion in Sec. VI C, we shall later introduce massive particles and compute their v_n in the "probe approximation," namely, by neglecting their backreaction to the flow velocity. Since we add in particles in the final state that do not exist in the fluid, the total energy is not conserved at freeze-out. But the fraction of the change $\delta\varepsilon/\varepsilon \sim e^{-m/T}$ is exponentially suppressed by the mass m and will be neglected.

The integral in (19) is taken over the hypersurface Σ of constant energy density where the kinetic freeze-out occurs. In the ideal case, constant ε means constant T since $\alpha = \mu/T$ is a constant. Let us write the condition of constant energy density as

$$\varepsilon(\tau, x_\perp, \phi) = T^4 f(\alpha) \equiv \frac{C^4 B^4}{(2L)^4} f(\alpha) = \varepsilon_c. \qquad (20)$$

Typically, ε_c is of the order of the critical energy density of the QCD phase transition. We take $\varepsilon_c = 1 \text{ GeV/fm}^3$ in this paper. Following [19], we assume that the condition (20) is reached within the early time regime $\tau \ll L$ where we can use the approximate solution (15). The parameter B in (20) is then related to the (position-dependent) freeze-out time τ_f as

$$\tau_f(x_\perp, \phi) = \frac{(2L)^5}{B^3(L^2 + x_\perp^2)^2} \left(1 - 3\epsilon_n \left(\frac{2Lx_\perp}{L^2 + x_\perp^2} \right)^n \cos n\phi \right). \qquad (21)$$

For consistency with our early freeze-out scenario, we must have $B^3 \gg 1$.

Under these assumptions, the integral (19) can be performed analytically and the integrated v_n is obtained from the formula

$$v_n = \frac{\int dp_T v_n(p_T) \frac{dN}{dY dp_T}}{\int dp_T \frac{dN}{dY dp_T}}. \qquad (22)$$

In the ideal case $\delta f = 0$, v_n does not depend on k since the factor $e^{k\mu/T} = e^{k\alpha}$ cancels in the ratio (22). The result is [19][2]

$$\frac{v_n}{\epsilon_n} = \frac{9}{64} \frac{\Gamma(3n)}{\Gamma(4n)} \left(\frac{128}{B^3} \right)^n \Gamma^2\left(\frac{n}{2} \right) \frac{n^2(3n+2)^2(n-1)}{2(4n+1)}$$

$$\sim B^{-3n} \propto \left(\frac{f^{3/4}}{\varepsilon_c^{3/4} L^3} \frac{dN}{dY} \right)^n. \qquad (23)$$

This determines the $\alpha = \mu/T$ dependence of v_n. Quite generally, $f(\alpha)$ is an increasing function α. On the other hand, dN/dY is a decreasing function of α. We shall see that, in heavy-ion collisions, the latter dependence is stronger, and as a result (23) is a decreasing function of α, or equivalently, an increasing function of the collision energy $\sqrt{s}$. Incidentally, we note that the directed flow $v_{n=1}$ vanishes, consistently with our assumption of boost invariance.

IV. VISCOUS CASE

We now turn to the viscous case $\eta, \kappa_i \neq 0$. Although the system is out of equilibrium, from the Landau matching condition we can define the local T and μ using the same relations as in equilibrium

$$\varepsilon = T^4 f\left(\frac{\mu}{T} \right), \qquad n = \mu T^2 g\left(\frac{\mu}{T} \right), \qquad \tilde{n} = \tilde{\mu} T^2 \tilde{g}\left(\frac{\mu}{T} \right), \qquad (24)$$

but now μ/T cannot be a constant.

A. Isotropic viscous solution

First consider the isotropic case $\hat{u}^\mu = \delta_\rho^\mu$. Although μ/T in (2) is not a constant anymore, it depends only on ρ (see below). Then we still have $\hat{J}^\mu = \hat{n}\delta_\rho^\mu$ so that

$$n \propto \frac{1}{\tau^3 \cosh^2 \rho} \qquad (25)$$

is the same as in the ideal case [17]. However, the solution of the Navier-Stokes equation ε_{NS} has an extra ρ-dependence proportional to the shear viscosity η. In the case of vanishing chemical potentials, this ρ-dependence can be obtained exactly [16],

---

[2]See (61) of [19]. We have corrected a mistake by a factor of 2 in the overall normalization. The same comment applies to (48) below.

$$\varepsilon_{\mathrm{NS}} = \frac{1}{\tau^4} \frac{fC^4}{(\cosh\rho)^{8/3}} \left[1 + \frac{\hat{\eta}}{9f^{1/4}C} \sinh^3\rho \, {}_2F_1\left(\frac{3}{2},\frac{7}{6},\frac{5}{2};-\sinh^2\rho\right) \right]^4, \tag{26}$$

where $\hat{\eta} \equiv \eta/\varepsilon_{\mathrm{NS}}^{3/4}$ is independent of ρ.

However, at finite density, $\hat{\eta}$ will depend on ρ, and this makes it difficult to find an exact solution. Related to this, η can now depend on both ε and n, and this relation can be model dependent. We can get around this problem by assuming that η is small. Specifically, we rescale η by the entropy density s,

$$\eta = \bar{\eta}\left(\frac{\mu}{T}\right) s, \tag{27}$$

as is often done in hydrodynamic simulations. We then regard $\bar{\eta}$ as a small parameter $[\bar{\eta} \sim \mathcal{O}(10^{-1})]$ and keep only terms linear in $\bar{\eta}$. In this approximation, we may replace μ/T and s in (27) by their equilibrium values at $\eta = 0$, namely, $\mu/T = \alpha$ and

$$s \approx \frac{1}{T_0}(\varepsilon_0 + p_0 - \mu_0 n_0) = \frac{C^3}{\tau^3 \cosh^2\rho}\left(\frac{4}{3}f(\alpha) - \alpha^2 g(\alpha)\right) \equiv \frac{C^3}{\tau^3 \cosh^2\rho} h(\alpha). \tag{28}$$

We then find the solution valid to $\mathcal{O}(\bar{\eta})$:

$$\begin{aligned}
\varepsilon_{\mathrm{NS}} = T^4 f\left(\frac{\mu}{T}\right) &\approx \frac{f(\alpha)C^4}{\tau^4(\cosh\rho)^{8/3}}\left[1 + \frac{4h(\alpha)\bar{\eta}(\alpha)}{9f(\alpha)C}\sinh^3\rho\,{}_2F_1\left(\frac{3}{2},\frac{7}{6},\frac{5}{2};-\sinh^2\rho\right)\right] \\
&\approx \frac{f(\alpha)C^4}{\tau^4(\cosh\rho)^{8/3}}\left[1 - \frac{2h(\alpha)\bar{\eta}(\alpha)}{f(\alpha)C}\left(\frac{e^{-\rho}}{2}\right)^{2/3}\right],
\end{aligned} \tag{29}$$

$$n_{\mathrm{NS}} = \mu T^2 g\left(\frac{\mu}{T}\right) = \frac{\alpha g(\alpha)C^3}{\tau^3\cosh^2\rho}, \tag{30}$$

where in the second line of (29) we focus on the early-time regime where ρ is negative and large.[3]

Using (29) and (30), we can eliminate C:

$$\frac{\left(\frac{\mu}{T}g\left(\frac{\mu}{T}\right)\right)^{4/3}}{f\left(\frac{\mu}{T}\right)} = \frac{(\alpha g(\alpha))^{4/3}}{f(\alpha)\left(1 - \frac{2h(\alpha)\bar{\eta}(\alpha)}{f(\alpha)C}\left(\frac{e^{-\rho}}{2}\right)^{2/3}\right)}. \tag{31}$$

Writing

$$\frac{\mu}{T} = \alpha + \delta\alpha(\rho), \tag{32}$$

we find the deviation from constancy due to the viscosity,

$$\delta\alpha(\rho) \approx \frac{2h\bar{\eta}}{Cf}\frac{\left(\frac{e^{-\rho}}{2}\right)^{2/3}}{\frac{4}{3\alpha} + \frac{4g'}{3g} - \frac{f'}{f}} = \gamma\frac{h\bar{\eta}}{Cf}\left(\frac{L^2 + x_\perp^2}{2L\tau}\right)^{2/3}, \tag{33}$$

where

$$\gamma(\alpha) \equiv \frac{2}{\frac{4}{3\alpha} + \frac{4g'}{3g} - \frac{f'}{f}}. \tag{34}$$

Note that $\gamma(\alpha) \propto \alpha$ as $\alpha \to 0$. At the freeze-out time $\tau = \tau_f$, we have the relation

$$\frac{\mu}{T} = \alpha + \delta\alpha|_{\text{freeze-out}} \approx \alpha + \gamma K\frac{(L^2 + x_\perp^2)^2}{(2L)^4}. \tag{35}$$

Finally, we can solve for T and μ using (32). The result is

$$\begin{aligned}
T &= \frac{C}{\tau(\cosh\rho)^{2/3}}\left(1 - \frac{\delta\alpha}{3}\left(\frac{1}{\alpha} + \frac{g'}{g}\right)\right), \\
\mu &= \frac{\alpha C}{\tau(\cosh\rho)^{2/3}}\left(1 + \frac{\delta\alpha}{3}\left(\frac{2}{\alpha} - \frac{g'}{g}\right)\right).
\end{aligned} \tag{36}$$

B. Anisotropic viscous solution

We now perturb the solution as in (15). First consider the current in (2). μ/T now depends not only on ρ, but also on

---

[3]The viscous Gubser solution is known to become unphysical (the temperature becomes negative) as $\rho \to -\infty$ [16]. Physically, this corresponds to very early times and/or very large values of $x_\perp$. Our results are not sensitive to these regions. We can simply choose the initial time of the evolution to be small, but not too small. Besides, all the $x_\perp$-integrals to be performed below are fully convergent at $x_\perp \to \infty$.

Θ and ϕ. However, the dependence is of order η. [See (43) below. Remember that for the ideal solution μ/T is constant even in the anisotropic case.] Therefore, if we neglect terms of order $\mathcal{O}(\kappa\eta\epsilon_n)$, we can approximate $\hat{J}^\mu \approx \hat{n}\hat{u}^\mu$. Then (18) is still valid and we get

$$n = \mu T^2 g\left(\frac{\mu}{T}\right) \approx \frac{\alpha g(\alpha)C^3}{\tau^3 \cosh^2\rho}(1 - \epsilon_n \mathcal{A})^3. \tag{37}$$

As for the energy density, we find

$$\varepsilon = T^4 f\left(\frac{\mu}{T}\right) \approx \frac{f(\alpha)C^4}{\tau^4(\cosh\rho)^{8/3}}\left(1 - \frac{2h(\alpha)\bar{\eta}(\alpha)}{f(\alpha)C}\left(\frac{e^{-\rho}}{2}\right)^{2/3}\right)(1 - \epsilon_n \mathcal{A}\delta)^4, \tag{38}$$

where [19]

$$\delta \approx 1 + \frac{h(\alpha)\bar{\eta}(\alpha)}{2f(\alpha)C}\left(\frac{e^{-\rho}}{2}\right)^{2/3}. \tag{39}$$

From the constant energy condition

$$\varepsilon = \frac{C^4 B^4}{(2L)^4}f(\alpha) = \varepsilon_c, \tag{40}$$

we can determine the freeze-out surface $\tau(x_\perp, \phi)$ in the viscous case [19],

$$\tau_f(x_\perp, \phi) = \frac{(2L)^5}{B^3(L^2 + x_\perp^2)^2}\left(1 - \frac{3K(L^2 + x_\perp^2)^2}{2(2L)^4} - 3\epsilon_n\left(\frac{2Lx_\perp}{L^2 + x_\perp^2}\right)^n \cos n\phi\right), \tag{41}$$

where the "Knudsen number" is proportional to the shear viscosity

$$K = \frac{h(\alpha)\bar{\eta}(\alpha)B^2}{f(\alpha)C}. \tag{42}$$

(32) and (36) are also modified as $\frac{\mu}{T} = \alpha + \delta\alpha'$ where

$$\delta\alpha' = \delta\alpha(1 + \epsilon_n \mathcal{A}) = \delta\alpha\left(1 + \epsilon_n\left(\frac{2Lx_\perp}{L^2 + x_\perp^2}\right)^n \cos n\phi\right), \tag{43}$$

and

$$T = \frac{C}{\tau(\cosh\rho)^{2/3}}\left[1 - \epsilon_n \mathcal{A} - \frac{\delta\alpha}{3}\left(\frac{1}{\alpha} + \frac{g'}{g}\right)\right], \qquad \mu = \frac{\alpha C}{\tau(\cosh\rho)^{2/3}}\left[1 - \epsilon_n \mathcal{A} + \frac{\delta\alpha}{3}\left(\frac{2}{\alpha} - \frac{g'}{g}\right)\right]. \tag{44}$$

C. v_n at finite μ and η

The computation of v_n is more complicated than the $\mu = 0$ case. This is because $\varepsilon = \text{const}$ does not mean $T = \text{const}$, and therefore one cannot treat T in the Boltzmann factor (19) as a constant when integrating over the hypersurface of constant energy. In order to cope with this, we write (44) as

$$T = T_c - \frac{T_0 f'}{4f}\delta\alpha, \tag{45}$$

where

$$T_c \equiv \frac{CB}{2L} = T_0\left(1 - \epsilon_n \mathcal{A} - \frac{h\bar{\eta}}{2fC}\left(\frac{L^2 + x_\perp^2}{2L\tau}\right)^{2/3}\right) \tag{46}$$

is constant by virtue of (40). We then expand the Boltzmann factor as[4]

---

[4]In this subsection we set $\tilde{\mu} = 0$. The case with $\tilde{\mu} \neq 0$ will be treated in the next subsection.

$$\exp\left(\frac{u \cdot p + k\mu}{T}\right) \approx e^{k\alpha} e^{u \cdot p/T_c} \exp\left[\delta\alpha\left(\frac{u \cdot p}{T_c^2}\frac{T_0 f'}{4f} + k(1 + \epsilon_n \mathcal{A})\right)\right]$$

$$\approx e^{k\alpha} e^{u \cdot p/T_c}\left\{1 + \delta\alpha\left(\frac{u \cdot p}{T_c}\frac{f'}{4f} + k\right)(1 + \epsilon_n \mathcal{A})\right\}, \tag{47}$$

where we approximated $T_c \approx T_0(1 - \epsilon_n \mathcal{A})$ in the $\mathcal{O}(\delta\alpha)$ term.

The first term in (47), proportional to unity, gives the same result as in [19],[5]

$$\frac{v_n}{\epsilon_n} = \frac{9}{64}\frac{\Gamma(3n)}{\Gamma(4n)}\left(\frac{128}{B^3}\right)^n \Gamma^2\left(\frac{n}{2}\right)\left\{\frac{n^2(3n+2)^2(n-1)}{2(4n+1)} - \frac{3n^3(n-1)K}{16(3n-1)}(3n^2 + 3n + 2)\right\}. \tag{48}$$

Note that $v_n/v_n^{\text{ideal}} = 1 - \mathcal{O}(nK)$ for $n \gg 1$ (see, however, [32]). The second term in (47) leads to a new order $\mathcal{O}(K)$ contribution to v_n. To compute it, we borrow some results from [19]. First, the perturbed flow velocity u^μ on the freeze-out surface has the following components in the coordinates (7):

$$u_\perp = u_{0\perp} + \delta u_\perp \epsilon_n \cos n\phi, \qquad u_\phi = \delta u_\phi \epsilon_n \sin n\phi, \tag{49}$$

where

$$u_{\perp 0} = 2x_\perp \frac{(2L)^5}{B^3(L^2 + x_\perp^2)^3},$$

$$\delta u_\perp = \frac{3(2L)^5}{B^3(L^2 + x_\perp^2)^4}\left(\frac{2Lx_\perp}{L^2 + x_\perp^2}\right)^{n-1}L(n(L^2 - x_\perp^2) - 4x_\perp^2),$$

$$\delta u_\phi = -\frac{3n}{2}\frac{(2L)^5}{B^3(L^2 + x_\perp^2)^2}\left(\frac{2Lx_\perp}{L^2 + x_\perp^2}\right)^n. \tag{50}$$

(The viscosity can be neglected here.) The exponential factor in the Boltzmann distribution reads

$$\frac{p \cdot u}{T_c} = \frac{1}{T_c}\left[-m_T \cosh(\zeta - Y) + p_T u_\perp \cos(\phi - \phi_p) - \frac{p_T u_\phi}{x_\perp}\sin(\phi - \phi_p)\right] \equiv U + \epsilon_n \delta U, \tag{51}$$

where $m_T = \sqrt{m^2 + p_T^2}$ is the transverse mass. The volume element of the constant energy hypersurface is

$$-p^\mu d\sigma_\mu = x_\perp \tau_f\left(m_T \cosh(\zeta - Y) - p_T \cos(\phi - \phi_p)\frac{\partial \tau_f}{\partial x_\perp} + \frac{p_T}{x_\perp}\sin(\phi - \phi_p)\frac{\partial \tau_f}{\partial \phi}\right)d\zeta dx_\perp d\phi, \tag{52}$$

where τ_f is given by (41) with the viscous term set to zero. Finally, we need the more precise version of (35)

$$\delta\alpha \approx \gamma K \frac{(L^2 + x_\perp^2)^2}{(2L)^4}(1 + 2\epsilon_n \mathcal{A}). \tag{53}$$

Armed with these formulas, let us decompose the contribution from the second term in (47) as

$$(2\pi)^3 \frac{dN}{dY p_T dp_T d\phi_p} \sim e^{k\alpha}\int_\Sigma (-p^\mu d\sigma_\mu)e^{U + \epsilon_n \delta U}\delta\alpha\left((U + \epsilon_n \delta U)\frac{f'}{4f} + k\right)(1 + \epsilon_n \mathcal{A})$$

$$\equiv (\delta J_1 + \delta J_2 + \delta J_3)\epsilon_n \cos n\phi_p, \tag{54}$$

corresponding to the three terms in (52). Consider δJ_1 first. To $\mathcal{O}(\epsilon_n)$ we have to evaluate

---

[5]For simplicity, here we ignore the contribution from the nonequilibrium part δf in (19). This has been computed in [19] for a particular choice of δf. However, its n-dependence is strongly affected by the choice of δf which is not unique [31]. Moreover, even the overall sign of this contribution is sensitive to the p_T-cutoff.

$$\delta J_1 \sim \epsilon_n \frac{2L\gamma K e^{k\alpha}}{B^3} m_T \int dx_\perp x_\perp \int d\zeta d\phi \cosh(\zeta - Y) e^U \delta U \left(\frac{f'}{4f} U + \frac{f'}{4f} + k \right). \tag{55}$$

This can be efficiently evaluated using the trick introduced in [19] [see Eq. (73) there]. The ϕ-integral gives Bessel functions $I_n(z)$ where

$$z \equiv \frac{p_T u_{\perp 0}}{T_c} = \frac{2x_\perp p_T (2L)^5}{T_c B^3 (L^2 + x_\perp^2)^3}. \tag{56}$$

This can be expanded as $I_n(z) \sim z^n$ anticipating that the subsequent p_T-integral is dominated by the region $z < 1$. We thus find

$$\begin{aligned}
\delta J_1 &\approx \frac{2L\gamma K e^{k\alpha}}{B^3} m_T \int_0^\infty dx_\perp x_\perp \frac{4\pi z^n}{2^n(n-1)!} \frac{1}{u_{\perp 0}} \left(\delta u_\perp - \frac{\delta u_\phi}{x_\perp} \right) \\
&\quad \times \left[\frac{f'}{4f} \left(nK_1(m_T/T_c) - \frac{m_T}{2T} (K_0(m_T/T_c) + K_2(m_T/T_c)) \right) + kK_1(m_T/T_c) \right] \\
&= \frac{2L\gamma K e^{k\alpha}}{B^3} 9\pi L^2 m_T \left(\frac{64 p_T}{T_c B^3} \right)^n \frac{n(n-1)\Gamma(3n)}{(3n-1)\Gamma(4n)} \\
&\quad \times \left[\frac{f'}{4f} \left(nK_1(m_T/T_c) - \frac{m_T}{2T} (K_0(m_T/T_c) + K_2(m_T/T_c)) \right) + kK_1(m_T/T_c) \right]. \tag{57}
\end{aligned}$$

The correction to v_n can be calculated from the formula [cf. (22)]

$$\delta v_n^1 \equiv \frac{\int_0^\infty dp_T p_T \delta J_1}{\int_0^\infty dp_T p_T J^0} \frac{\epsilon_n}{2}, \tag{58}$$

where J^0 is the azimuthally symmetric part [cf. Eq. (45) of [19]],

$$J^0 = 4\pi m_T K_1(m_T/T_c) \frac{16L^3}{B^3} e^{k\alpha}. \tag{59}$$

In the massless case $m_T = p_T$, the integral can be done exactly and we find

$$\begin{aligned}
\frac{\delta v_n^1}{\epsilon_n} &= \frac{9\gamma K}{128} \left(k - \frac{3f'}{4f} \right) \left(\frac{128}{B^3} \right)^n \frac{n^2(n-1)\Gamma(3n)}{(3n-1)\Gamma(4n)} \\
&\quad \times \Gamma\left(\frac{n}{2} + 2 \right) \Gamma\left(\frac{n}{2} \right), \tag{60}
\end{aligned}$$

and from (23),

$$\frac{\delta v_n^1}{v_n^{\text{ideal}}} = \frac{\gamma K}{4} \left(k - \frac{3f'}{4f} \right) \frac{n(n+2)(4n+1)}{(3n-1)(3n+2)^2}. \tag{61}$$

It is important to emphasize that (61) is induced by the combined effect of the chemical potential and the viscosity. It vanishes when $\eta = 0$ or $\alpha = \mu/T = 0$ because $\gamma(0) = 0$

[cf. (34)]. Compared with (48) which schematically reads $\delta v_n / v_n^{\text{ideal}} \sim -nK$, we notice that (61) is not enhanced by a factor of n, hence subleading at large n. However, it is the leading contribution to the *difference* in v_n between particles ($k = 1$) and antiparticles ($k = -1$). If $\mu = \mu_B > 0$ is the baryon chemical potential, the protons have larger v_n than the antiprotons. We shall study this effect in detail later.

In fact, for protons the approximation $m_T \approx p_T$ is not valid. Instead, we now assume $m_T \gg T$ and reevaluate δv_n. Note that when $m_T \gg T$, δJ_1 is parametrically larger than $\delta J_{2,3}$, so it is enough to consider only δJ_1.

When $m_T \gg T$, the Bessel function is independent of the order

$$K_i(m_T/T_c) \approx \sqrt{\frac{\pi T_c}{2m_T}} e^{-m_T/T_c}, \tag{62}$$

so that (57) becomes

$$\begin{aligned}
\delta J_1 &\approx \frac{2\gamma K e^{k\alpha}}{B^3} 9\pi L^3 m_T \left(\frac{64 p_T}{T_c B^3} \right)^n \frac{n(n-1)\Gamma(3n)}{(3n-1)\Gamma(4n)} K_1(m_T/T_c) \\
&\quad \times \left[\frac{f'}{4f} \left(n - \frac{m_T}{T_c} \right) + k \right]. \tag{63}
\end{aligned}$$

On the other hand, from Eq. (47) of [19],

$$\delta J_1^{\text{ideal}} = 4\pi e^{k\alpha} \frac{m_T}{B^3} K_1(m_T/T_c) \frac{\Gamma(3n)}{\Gamma(4n)} 9L^3 \left(\frac{64 p_T}{T_c B^3}\right)^n (n-1) \frac{2(3n+2)}{4n+1}. \tag{64}$$

The p_T-integral can be evaluated by the saddle point at $p_T^* = \sqrt{nmT_c}$ for $m \gg nT_c$ and we obtain

$$\frac{\delta v_n^1}{v_n^{\text{ideal}}} \approx \frac{\gamma K}{4} \frac{n(4n+1)}{(3n-1)(3n+2)} \left(\frac{f'}{4f}\left(\frac{n}{2}-\frac{m}{T_c}\right) + k\right). \tag{65}$$

The k-independent part is order $\frac{m}{T} K \gg nK$, but we shall see later that it is numerically small for realistic values of m because the factor $\gamma f'/f$ is small. The k-dependent term is again of order $\mathcal{O}(K)$ without an enhancement by a factor of n.

The evaluation of $\delta J_{2,3}$ in (54) can be done similarly, though it is considerably more tedious. Here we only show the final result in the massless case $m = 0$, relegating the details to the Appendix:

$$\frac{\delta v_n^{2+3}}{\epsilon_n} = \frac{9\gamma K}{128}\left(k - \frac{3f'}{4f}\right)\left(\frac{128}{B^3}\right)^n \frac{n^3(n-1)\Gamma(3n)}{(3n-1)\Gamma(4n)}\Gamma\left(\frac{n}{2}+1\right)\Gamma\left(\frac{n}{2}\right). \tag{66}$$

Comparing with (60), we notice that $\delta v_n^1 = \frac{n+2}{2n}\delta v_n^{2+3}$. Actually, this relation was repeatedly observed in [19] when computing other contributions to v_n. We do not have a simple explanation for this.

Summing all the contributions including the previously computed term [19], our final result of the viscous correction δv_n in the massless case is

$$\frac{\delta v_n}{\epsilon_n} = \frac{K}{256}\frac{\Gamma(3n)}{\Gamma(4n)}\left(\frac{128}{B^3}\right)^n\Gamma^2\left(\frac{n}{2}\right)\frac{n^3(n-1)}{3n-1}\left\{-\frac{27}{4}(3n^2+3n+2) + 9\gamma\left(\frac{3n}{2}+1\right)\left(k-\frac{3f'}{4f}\right)\right\}. \tag{67}$$

The second term in the curly brackets is the new contribution at finite density. It is subleading in n, and actually the factor $\gamma(\alpha)$ is also numerically small. However, it gives the leading contribution to the difference in v_n between particles and antiparticles.

D. Isospin chemical potential

In the previous subsection, we computed v_n of particles which couple to the "large" chemical potential μ. Here let us compute v_n of particles neutral under μ but charged under $\tilde{\mu}$. We have in mind the charged pions $\pi^\pm$ in the presence of the isospin chemical potential. We start with the formula [cf. (37)]

$$\tilde{n} = \frac{\tilde{\alpha}\,\tilde{g}(\alpha)C^3}{\tau^3\cosh^2\rho}(1-\epsilon_n\mathcal{A})^3 = \tilde{\mu}T^2\tilde{g}(\mu/T). \tag{68}$$

We treat $\tilde{\alpha} = \tilde{\mu}/T$ as a small parameter and keep only terms linear in $\tilde{\alpha}$. Dividing by T^3 from (44) and using $\mu/T = \alpha + \delta\alpha(1 + \epsilon_n\mathcal{A})$, we find

$$\frac{\tilde{\mu}}{T} = \frac{\tilde{\alpha}\,\tilde{g}(\alpha)(1-\epsilon_n\mathcal{A})^3}{\tilde{g}(\mu/T)\left(1-\epsilon_n\mathcal{A}-\frac{\delta\alpha}{3}\left(\frac{1}{\alpha}+\frac{g'}{g}\right)\right)^3} \approx \tilde{\alpha}\left(1+\delta\alpha\left(\frac{1}{\alpha}+\frac{g'}{g}-\frac{\tilde{g}'}{\tilde{g}}\right)(1+\epsilon_n\mathcal{A})\right). \tag{69}$$

The fugacity factor thus becomes

$$e^{k\tilde{\mu}/T} \approx e^{k\tilde{\alpha}}\left(1 + k\tilde{\alpha}\delta\alpha\left(\frac{1}{\alpha}+\frac{g'}{g}-\frac{\tilde{g}'}{\tilde{g}}\right)(1+\epsilon_n\mathcal{A})\right). \tag{70}$$

As before, the factor $e^{k\tilde{\alpha}}$ drops out in the computation of v_n. We see that the only difference from the previous case (47) is that k is replaced by

$$k\frac{\tilde{\alpha}}{\alpha}\left(1 + \frac{\alpha g'}{g} - \frac{\alpha\tilde{g}'}{\tilde{g}}\right). \tag{71}$$

Thus the final result is the same as (67) except that k is replaced by (71).

V. PHENOMENOLOGICAL INPUTS

This section serves as a preparation for the next section where we compare our results with the experimental data.

A. Models

In order to make quantitative predictions, we need models for the functions f, g, $\tilde{g}$ defined in (5). Here we consider two extreme scenarios in terms of the interaction strength.

1. Free quark-gluon gas

The energy density of free, massless three flavor QCD is

$$\varepsilon = 3p = \frac{8\pi^2}{15}T^4 + 6\sum_{q=u,d,s}\left(\frac{7\pi^2}{120}T^4 + \frac{\mu_q^2 T^2}{4} + \frac{\mu_q^4}{8\pi^2}\right),$$

$$n_q = \frac{\partial p}{\partial \mu_q} = \mu_q T^2\left(1 + \frac{\mu_q^2}{\pi^2 T^2}\right), \tag{72}$$

where $\mu_u = \frac{\mu_B}{3} + \frac{\mu_I}{2}$, $\mu_d = \frac{\mu_B}{3} - \frac{\mu_I}{2}$ and $\mu_s = \frac{\mu_B}{3} - \mu_S$. μ_B, μ_I and μ_S are the baryon, isospin and strangeness chemical potentials, respectively. Since the net strangeness is zero in heavy-ion collisions, we set $\mu_S = \mu_B/3$ and obtain ($\alpha = \mu_B/T$)

$$f(\alpha) = \frac{19}{12}\pi^2 + \frac{\alpha^2}{3} + \frac{\alpha^4}{54\pi^2}, \tag{73}$$

$$g(\alpha) = g_B(\alpha) = 2\left(1 + \frac{\alpha^2}{9\pi^2}\right),$$

$$\tilde{g}(\alpha) = g_I(\alpha) = \frac{1}{2}\left(1 + \frac{\alpha^2}{3\pi^2}\right). \tag{74}$$

It turns out that, due to the large denominators $9\pi^2$ or $3\pi^2$, the effect of g and $\tilde{g}$ on v_n is numerically small.

2. $\mathcal{N} = 4$ SYM at finite $\mathcal{R}$-charge chemical potential

Next we consider strongly coupled $\mathcal{N} = 4$ supersymmetric Yang-Mills theory at finite R-charge chemical potential μ. This theory is conformal, and in the limit of strong coupling and at large N_c, the thermodynamic quantities can be computed from the AdS/CFT correspondence. The results are [33]

$$\varepsilon = 3p = \frac{3\pi^2 N_c^2 T^4}{8}\frac{1}{2^4}\left(\sqrt{1 + \frac{2\mu^2}{3\pi^2 T^2}} + 1\right)^3$$

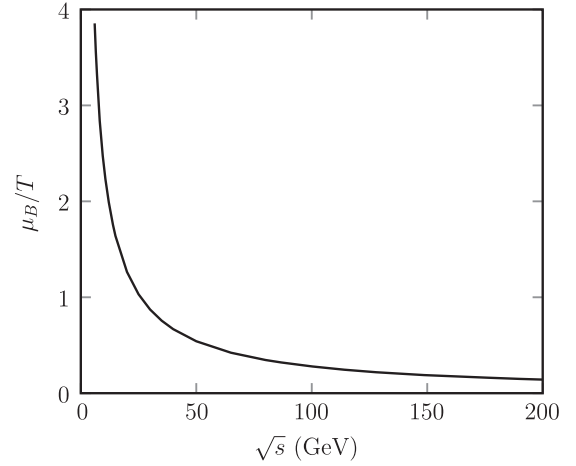$$\times \left(3\sqrt{1 + \frac{2\mu^2}{3\pi^2 T^2}} - 1\right), \tag{75}$$

FIG. 1. μ_B/T at freeze-out as a function of the collision energy $\sqrt{s}$ (per nucleon).

$$n = \frac{\partial p}{\partial \mu} = \frac{\mu N_c^2 T^2}{16}\left(\sqrt{1 + \frac{2\mu^2}{3\pi^2 T^2}} + 1\right)^2, \tag{76}$$

where n is the R-charge density. The shear viscosity is given by $\eta = \frac{s}{4\pi}$.

There are uncertainties when treating this model as a proxy of strongly coupled QCD, such as the value of N_c and the proportionality constant between μ and μ_B. However, in practical fits, the normalization of $f \propto N_c^2$ can be absorbed by a change in L [cf. Eq. (20)]. Moreover, as long as $\mu \sim \mathcal{O}(\mu_B)$, the two functions (73) and (75) are qualitatively not so different in shape for $\mu \sim \mathcal{O}(T)$. As a result, the quality of fits is similar in the two cases despite the huge differences in the underlying dynamics. Therefore, in the next section we show only the results based on (73) and (74).

B. Freeze-out conditions

We employ the following phenomenological parametrization [34] of the freeze-out temperature T and chemical potential μ_B (in units of GeV) as a function of the collision energy $\sqrt{s}$ (per nucleon, in units of GeV):

$$T(\mu_B) = a - b\mu_B^2 - c\mu_B^4, \qquad \mu_B = \frac{d}{1 + e\sqrt{s}}, \tag{77}$$

with $a = 0.166$, $b = 0.139$, $c = 0.053$, $d = 1.308$, $e = 0.273$. This gives μ_B/T as a function of $\sqrt{s}$ as shown in Fig. 1. The curve is well approximated by $\mu_B/T \approx d/(ae\sqrt{s}) \approx 29/\sqrt{s}$. Actually, T and μ_B here are the *chemical* freeze-out parameters which are in general different from those entering the Cooper-Frye formula (19) used at the *kinetic* freeze-out. However, in our model only the ratio μ_B/T matters, and this ratio is roughly constant as

we have seen. We thus use the relation in Fig. 1 for the evaluation of v_n.

The parameter C also depends on $\sqrt{s}$ via (14). We use the following empirical formula for the charged particle multiplicity [35]

$$\frac{dN_{ch}}{dY} \approx 2\frac{4C^3}{\pi} \approx 148(\sqrt{s})^{0.3}, \qquad (78)$$

where the factor of 2 counts the degeneracy between π^+ and π^-. From (40) and (78), we see that the Knudsen number (42) behaves as

$$K \approx \frac{8h\bar{\eta}L^2\sqrt{5\epsilon_c}}{37\pi f^{3/2}(\sqrt{s})^{0.3}} \sim \frac{\bar{\eta}L^2}{f^{1/2}(\sqrt{s})^{0.3}} \sim \frac{\bar{\eta}(\mu_B/T)^{0.3}}{\sqrt{1 + \#(\mu_B/\pi T)^2}}, \qquad (79)$$

where L is in units of fermi and $\epsilon_c = 1$ is in units of GeV/fm^3. Putting aside the potential μ_B-dependence of $\bar{\eta} = \eta/s$, we see that K is an increasing function of μ_B (up to $\mu_B \lesssim \pi T$ in our model) or a decreasing function of $\sqrt{s}$.

In fact, up to the RHIC energy, we find that the following parametrization also gives a good description of the data [36],

$$\frac{dN_{ch}}{dY} = 72 \ln \frac{(\sqrt{s})^2}{1.41}. \qquad (80)$$

We shall also use this in Sec. VI B.

VI. COMPARISON WITH THE EXPERIMENTAL DATA

In this section, we compare our results with three different experimental data: (i) the n-dependence of v_n measured at the LHC; (ii) the collision energy dependence of v_2 measured at the SPS; (iii) the difference in v_2 between particles and antiparticles measured at RHIC.

A. Higher harmonics v_n

The CMS collaboration at the LHC has measured the p_T-integrated v_n in lead-lead collisions at $\sqrt{s} = 2.76$ TeV up to rather high orders ($n \le 7$) [37]. Using (23) and (67) together with the phenomenological inputs in the previous section, we can evaluate v_n and compare with the CMS data.[6] The result is shown in Fig. 2. Here we set $\epsilon_n = 0.018$ for all different values of n. Taking ϵ_n to be independent of n may be a good approximation for the very central (0%–0.2% centrality) nucleus collisions.[7] The parameter L is set

---

[6]The CMS uses the p_T cuts $0.3 < p_T < 3$ GeV while our analytical result is integrated over all p_T. We checked that the quality of the fit is unchanged by introducing cuts in our model.

[7]The value 0.018 may seem a bit too small. This may be due to our nonstandard definition of ϵ_n (17).
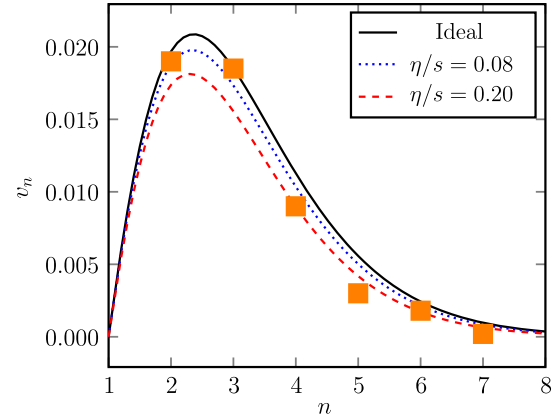

FIG. 2 (color online). v_n versus different values of n from 2 to 7 measured by the CMS collaboration (0%–0.2% centrality) [37]. The black solid curve represents the ideal hydrodynamic result, while the blue dotted curve and red dashed curve correspond to the viscous results with $\eta/s = 0.08$ and $\eta/s = 0.2$, respectively. See, also, Ref. [32].

to 17 fm. The corresponding value of B in (48) is $B^3 \approx 26.7$ which is consistent with the assumption $B^3 \gg 1$.

As a matter of fact, since $\mu_B \approx 0$ at the LHC, the new term at $\mu_B > 0$ [the term proportional to γ in (67)] is negligibly small, and the present fit could have been done in [19] treating B as a fitting parameter. By expressing B in terms of observables as we have done here, we can test our result at lower energies or higher chemical potentials $\mu_B \sim \mathcal{O}(T)$. Note that since B^3 is larger at lower energies, $v_n \sim e^{-n\ln(4B^3/27)}$ [19] decreases faster with n, and this will make the measurement of higher harmonics difficult at low energies [38].

B. Energy dependence of v_2

Next we turn to the energy dependence of the elliptic flow $v_{n=2}$ for which there are already a wealth of experimental data from the SPS and the RHIC BES program [28,39]. We compare our formulas (48) and (67) (with $k = 0$) for $n = 2$ with the SPS, midcentral data collected in the low energy region $\sqrt{s} < 20$ GeV [28,36].[8] The result with three different values of η/s is shown in Fig. 3 where we tried both (78) and (80), the latter actually gives a better description of dN_{ch}/dY in this low energy region. The other parameters are chosen as $L = 15.5$ fm and $\epsilon_2 = 0.32$. The value of L here is slightly smaller than the one ($L = 17$ fm) used in Fig. 2. This is consistent with the perception that the QGP droplet is larger at higher energies at the time of thermalization. The rise of v_2 with energy is nicely reproduced by our formula and attributed to the rise of dN_{ch}/dY. It turns out that the newly calculated viscous

---

[8]The SPS data do not have a low-p_T cutoff while the RHIC data have $p_T > 0.2$ GeV. Our analytical formula, integrated over all p_T, should fare better with the SPS results.
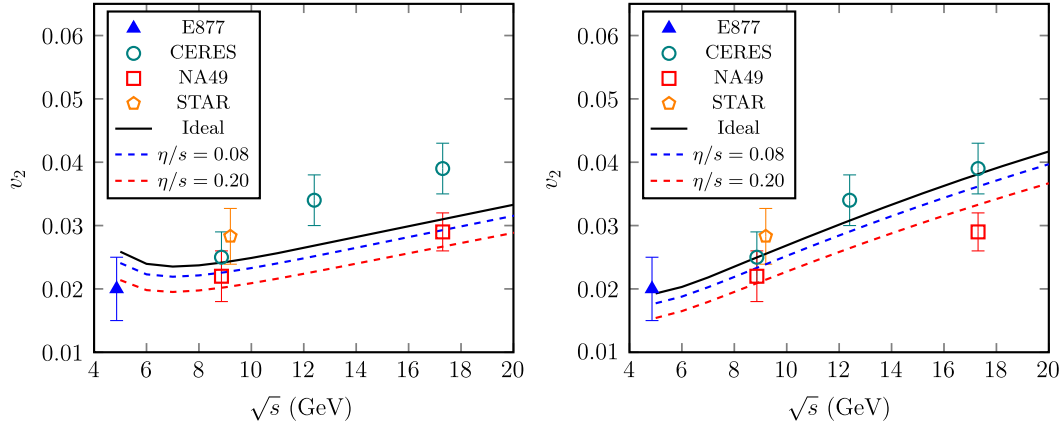
FIG. 3 (color online).   The energy dependence of v_2 compared with the SPS data [36] for midcentral collisions. We used (78) and (80) in the left and right plots, respectively.

correction in Sec. IV C [the last term in (67)] is numerically very small [about an order of magnitude smaller than the first term in (67)] even in the highest density region.

Unfortunately, this fit, which agrees reasonably well with the low energy data, overshoots the high energy RHIC data at $\sqrt{s} = 200$ GeV [40,41] in similar centrality bins by a factor of 2 (assuming that ϵ_2 is independent of energy). This is because the rise of dN/dY with energy is too steep. If we artificially reduce the exponent in (78) as $0.3 \rightarrow 0.23$, for example, we get a decent description of v_2 over a broader range in $\sqrt{s}$.[9] Alternatively, the dependence $v_2 \sim (dN/dY)^2$ from (23) may be too strong, and the experimental data actually suggest a weaker dN/dY-dependence [28]. While we do not have a resolution of this problem in the present framework, it seems qualitatively correct that v_2 is directly proportional to the multiplicity to some positive power, and therefore it is an increasing function of $\sqrt{s}$ (see, also, Sec. VII of [19]).

C. Difference in v_n between particles and antiparticles

Finally, we investigate the difference in v_2 between particles and antiparticles which has been measured by the STAR collaboration at RHIC [13,14] and attracted some attention from theoretical viewpoints [42–45]. For a hadron with the quantum numbers $(\mathcal{B}, I, S)$ (baryon number, isospin, strangeness), we assign the fugacity factor

$$\exp\left(\frac{\mathcal{B}\mu_B + I\mu_I + S\mu_S}{T}\right). \tag{81}$$

($S = -1$ for the strange quark.) In heavy-ion collisions, $\mu_I < 0$ since the colliding nuclei are neutron rich, and $\mu_S \approx \mu_B/3$ since the net strangeness vanishes. The latter condition implies that we should not treat μ_S as a small

perturbation. Indeed, various estimates of $r_S \equiv \mu_S/\mu_B$ based on the SPS [46] and RHIC [47] data, and also from lattice QCD [48,49] all found similar values within the range $0.21 < r_S < 0.27$. We thus regard μ_S as a shift of μ_B for strange hadrons and treat it as a fitting parameter, anticipating that the value of r_S should come out in the window $0.2 < r_S < 1/3$. On the other hand, we regard $r_I \equiv \mu_I/\mu_B$ as a small parameter compared to unity and use the result obtained in Sec. IV D.

Let us define the difference in v_n between hadrons X and antihadrons $\bar{X}$ as

$$\Delta v_n^X \equiv v_n^X - v_n^{\bar{X}}. \tag{82}$$

This can be evaluated from (67) and (71). Focusing now on the elliptic flow case $n = 2$, we can immediately write down the following "master formula":

$$\Delta v_2^X = \epsilon_2 \frac{6144}{35B^6}\gamma K\left[\mathcal{B} + r_S S + r_I I\left(1 + \frac{\alpha g'}{g} - \frac{\alpha g_I'}{g_I}\right)\right]. \tag{83}$$

By construction, (83) has been derived for massless particles. In the massive case, we observe that the following ratio,

$$\frac{\Delta v_2^X}{v_2^{X,\text{ideal}}} = \frac{9\gamma K}{40}\left[\mathcal{B} + r_S S + r_I I\left(1 + \frac{\alpha g'}{g} - \frac{\alpha g_I'}{g_I}\right)\right], \tag{84}$$

is exactly independent of m.[10] This is due to the nontrivial cancellation of p_T-integrals such as (58) in the ratio for the

---

[9]Note that (78) is for central collisions. The exponent may indeed be smaller for midcentral collisions.

[10]As already noted in Sec. III C, we introduce massive particles in the probe approximation, namely, we let these particles flow with the same flow velocity and neglect their backreaction to the velocity. While this causes some inconsistencies such as energy nonconservation, we expect that the essential features of (84) (the proportionality to the viscosity, μ's and the corresponding quantum numbers) are robust.
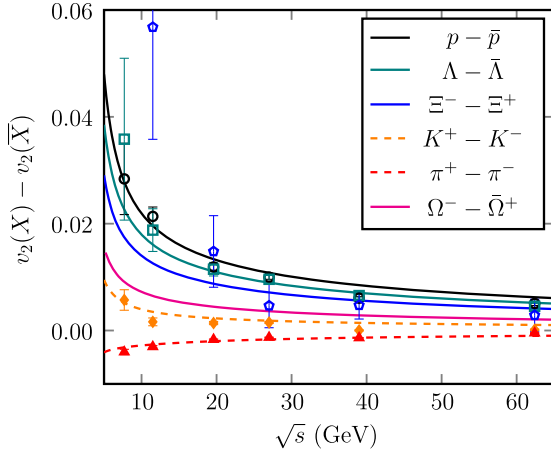
FIG. 4 (color online). $\Delta v_2^X \equiv v_2(X) - v_2(\bar{X})$ as a function of $\sqrt{s}$ compared with the STAR data for five different species of hadrons [13,14]. We use open symbols for baryons and filled symbols for mesons. The color of data points is chosen to match the color of the corresponding line for each hadron species. We have used $\eta/s = 0.2$, $\mu_S = 0.23\mu_B$ and $\mu_I = -0.15\mu_B$.

k-dependent part. In order to get Δv_2 itself, we must multiply (84) by [19],

$$v_2^{\text{ideal}} = \epsilon_2 \frac{2^{11}}{35 B^6 T} \frac{\int dp_T p_T^3 (\frac{m_T}{T} K_1(m_T/T) + 4 K_0(m_T/T))}{\int dp_T p_T m_T K_1(m_T/T)}. \tag{85}$$

The m-dependence of (85) is sensitive to the cutoffs of the p_T-integral, but overall the dependence is not very strong. For simplicity, in this study we ignore the m-dependence of v_2^{ideal} and use (83) for all hadron species. It is not difficult to implement this mass effect, but there are other subtleties which are not taken into account, either.[11] Clearly, it is desirable that the experimental results are plotted in the form (84) in order to avoid various systematic uncertainties.

The most important feature of (83) or (84) is that Δv_2 is proportional to *both* the shear viscosity η and the chemical potentials. [Remember that γ as defined in (34) is roughly proportional to μ_B.] This in particular means that Δv_2^π can be nonzero in viscous hydrodynamics in the presence of the isospin chemical potential.

Let us confront (83) with the data. The STAR collaboration has measured Δv_2^X for $X = \pi^+$, K^+, p, Λ, Ξ^- [13,14]. This is plotted in Fig. 4 together with our fit based on (83) with $\eta/s = 0.2$. We have used $L = 15.5$ fm and $\epsilon_2 = 0.32$ as in Fig. 3, and used the fit parameters $r_S = 0.23$ and $r_I = -0.15$, the former is consistent with our expectation mentioned above. The steep rise of Δv_2^X for

baryons towards the low-$\sqrt{s}$ region is due to the rough proportionality $\Delta v_2 \propto \gamma \propto \mu_B$. Compared to this, the μ_B-dependence of the factor $1/B^6$ is subleading. Since p, Λ, Ξ^-, K^+ have $(\mathcal{B}, I, S) = (1, \frac{1}{2}, 0)$, $(1, 0, -1)$, $(1, -\frac{1}{2}, -2)$, $(0, \frac{1}{2}, 1)$, respectively, we expect the ordering $\Delta v_2^p > \Delta v_2^\Lambda > \Delta v_2^{\Xi^-} > \Delta v_2^{K^+} > 0$ for reasonable values of $r_S > 0$ and $r_I < 0$. This tendency is obeyed by most data points except a few in the low energy region. We note that the Ξ^- data point at $\sqrt{s} = 11.5$ GeV should not be taken seriously because, according to the STAR collaboration [14], this data point is afflicted with "additional systematic effects which are not included in the error bars." In Fig. 4, we have also included our prediction for the Ω-baryon. Since Ω^- has $S = -3$, we expect that $\Delta v_2^\Omega \sim \mu_B - 3\mu_S$ is smaller than other baryons.[12]

Concerning the pions, the negative $\Delta v_2^{\pi^+}$ can be naturally explained by the negative isospin chemical potential. However, the magnitude is problematic. Our choice $r_I = -0.15$, which describes the pion data very well, is too large compared with the value $r_I \approx -0.02 \sim -0.03$ extracted from the SPS data [46,50]. We may dial r_I down to, say, $r_I \approx -0.1$ without spoiling much the quality of the $\Delta v_2^{\pi^+}$ fit, but not further down. On the other hand, the other hadrons (p, Λ, Ξ^-, K^+) are more or less unaffected by r_I and can be well fitted even with $r_I = -0.02$ and $r_S \approx 0.2$. This may be an indication that there are other mechanisms to generate the difference Δv_2 which predominantly act on the pions.[13]

In the large-$\sqrt{s}$ region, our result tends to slightly overestimate Δv_2^X. This is partly due to the too fast rise of v_2^{ideal} with energy as mentioned before. However, in Fig. 4 we assumed that $\eta/s = 0.2$ is independent of $\sqrt{s}$. A recent hydrodynamic simulation suggests that η/s is a decreasing function of $\sqrt{s}$ [27], and this could alleviate the (small) discrepancy in the large-$\sqrt{s}$ region (remember that $\Delta v_2^X \propto \eta/s$).

VII. SUMMARY AND CONCLUSIONS

In this paper, we have revealed, in a completely analytical manner, a number of interesting features about the nature of hydrodynamics in the presence of conserved currents as well as the chemical potential (collision energy) dependence of the flow harmonics v_n. Let us summarize the main findings.

(i) As a generalization of the Gubser flow [16], we have derived an anisotropic solution of the relativistic Navier-Stokes equation coupled with conserved

---

[11]For instance, the STAR collaboration uses 0%–80% centrality events to measure Δv_2. This reduces the effective value of μ_B by about 20% [14] and partly cancels the above mass effect for baryons when computing Δv_2.

[12]Multistrange hadrons such as Ω and Ξ may freeze out earlier than nonstrange hadrons. Again this uncertainty mostly goes away in the ratio (84).

[13]It is worth mentioning that feed-down corrections (resonance decays) are not included in the current estimates and they could change the fitting parameters.

currents. Conformal symmetry and boost invariance have been assumed. The solution is valid to linear order in the shear viscosity η and the eccentricity ϵ_n. Based on the solution and the Cooper-Frye formula, we analytically computed the flow harmonics v_n at finite density.

(ii) In ideal hydrodynamics, the QGP fireball follows a straight line trajectory $\mu/T = \text{const.}$ in the phase diagram in the (T, μ)-plane. The shear viscosity causes a deviation from the straight line as shown in (32). We expect this picture to be approximately correct in QCD in the deconfined phase of the hydroevolution.

(iii) v_n is a decreasing function of density (or an increasing function of $\sqrt{s}$) and decreases faster with n at higher densities $v_n \sim e^{-n \ln(4B^3/27)}$. This is because the lifetime of the hydrodynamic regime ($\sim 1/B^3$) is shorter at high density as it is correlated with the multiplicity $C^3 \sim dN/dY$ through the constant energy condition (20). In this regard, it is interesting to recall that in an early numerical study [23], a constant (or even decreasing) v_2 as a function of $\sqrt{s}$ was obtained if the hydrosimulation is continued to very low temperatures (the so-called "hydro limit" [51]). The rising v_2 with energy can be obtained by switching off hydrodynamics at a relatively high temperature [24]. Our assumption of early freeze-out is similar in spirit to this.

(iv) At finite chemical potential, there are new viscous corrections to v_n [the last terms proportional to γ in (67)]. Numerically, they are smaller than the contribution previously found in the $\mu = 0$ case [19]. However, they give the leading order contribution to the *difference* in v_n between particles and antiparticles.

(v) The viscous corrections to v_n are enhanced at high density. Even if η/s is constant, the Knudsen number K grows at high density as it is inversely proportional to the multiplicity (79). At large-n, it is also enhanced linearly by n, $v_n/v_n^{\text{ideal}} \sim 1 - \mathcal{O}(nK)$ [19].

(vi) The elliptic flow difference between particles and antiparticles $\Delta v_2^X = v_2^X - v_2^{\bar{X}}$ (or more generally, Δv_n^X) can be nonzero only if the particle X is charged under some chemical potential(s) *and* the shear viscosity is nonvanishing. This is related to the deviation from constancy of the ratio μ/T due to viscous effects. Our result is summarized by the master formula (83) [or the more fundamental formula (84)] which schematically reads $\Delta v_2^X \propto \eta \mu^X$.

This formula dictates the ordering $\Delta v_2^p > \Delta v_2^\Lambda > \Delta v_2^{\Xi^-} > \Delta v_2^{K^+} > 0 > \Delta v_2^{\pi^+}$ which seems to be borne out by the STAR result except for a few data points. Our mechanism of generating Δv_2^X is distinct from the previous theoretical considerations in [42,44], but we find it has some common ground with the discussion in [43]. Finally we pointed out that the observed magnitude of $\Delta v_2^{\pi^+}$ is large and can be fitted only if we assume an unnaturally large value of the isospin chemical potential μ_I. This suggests that other mechanisms to generate Δv_2^π may be at work.

Presumably some of the above features are empirically well known to the experts of hydrodynamic simulations. However, they have not been systematically derived with the level of analytical detail presented in this paper.

There are a number of directions for future work. Admittedly, the assumptions of boost invariance and conformal invariance are too simplistic, especially at high density. One has to relax these approximations to be more realistic. Related to this, we only considered the conformal equation of state $\varepsilon = 3p = T^4 f(\mu/T)$ where the function f does not carry any information about the crossover and possibly first order phase transitions at finite density. (Nevertheless it is remarkable that we can explain many features of v_n measured at different energies without such information.) It is important to figure out how the presence of phase transitions in f is encoded in the observed behavior of v_n. Including the effects of anomaly (see, e.g., [45]) is also interesting. We hope to address these questions in future work.

ACKNOWLEDGMENTS

APPENDIX: COMPUTATION OF $\delta J_{2,3}$

In this Appendix, we carry out the computation of $\delta J_{2,3}$ defined in (54). We first note that the last two terms of (52) may be combined as

$$-p_T \cos(\phi - \phi_p) \frac{\partial \tau}{\partial x_\perp} + \frac{p_T}{x_\perp} \sin(\phi - \phi_p) \frac{\partial \tau}{\partial \phi} \to \frac{(2L)^5 p_T}{B^3(L^2 + x_\perp^2)^3} \left[4x_\perp \cos\phi + 3\epsilon_n \left(\frac{2Lx_\perp}{L^2 + x_\perp^2} \right)^n \right.$$
$$\left. \times \left\{ \left(-4x_\perp + n \frac{L^2 - x_\perp^2}{x_\perp} \right) \cos n(\phi + \phi_p) \cos\phi + n \frac{L^2 + x_\perp^2}{x_\perp} \sin n(\phi + \phi_p) \sin\phi \right\} \right], \tag{A1}$$

where we shifted the integration variable ϕ as $\phi \rightarrow \phi + \phi_p$. We then make the following replacement:

$$\cos n(\phi + \phi_p)\cos\phi \rightarrow \cos n\phi \cos\phi \cos n\phi_p \rightarrow \frac{1}{2}\cos(n-1)\phi \cos n\phi_p,$$

$$\sin n(\phi + \phi_p)\sin\phi \rightarrow \sin n\phi \sin\phi \cos n\phi_p \rightarrow \frac{1}{2}\cos(n-1)\phi \cos n\phi_p, \tag{A2}$$

where we neglected $\sin n\phi_p$ which will vanish after the ϕ-integral, and also $\cos(n+1)\phi$ which will lead to subleading terms $I_{n+1}(z) \sim z^{n+1}$ after the ϕ-integral compared to $I_{n-1}(z) \sim z^{n-1}$. Thus, (A1) effectively becomes

$$\frac{(2L)^5 p_T}{B^3(L^2 + x_\perp^2)^3}\left[4x_\perp\cos\phi + 3\epsilon_n\left(\frac{2Lx_\perp}{L^2 + x_\perp^2}\right)^n\left(-2x_\perp + \frac{nL^2}{x_\perp}\right)\cos(n-1)\phi\cos n\phi_p\right]. \tag{A3}$$

Similarly, we can write δU defined in (51) as

$$\delta U \rightarrow \frac{p_T}{T_c}\left(\delta u_\perp \cos\phi \cos n(\phi + \phi_p) - \frac{\delta u_\phi}{x_\perp}\sin\phi \sin n(\phi + \phi_p)\right)$$

$$\rightarrow \frac{z}{2}\frac{1}{u_{\perp 0}}\left(\delta u_\perp - \frac{\delta u_\phi}{x_\perp}\right)\cos(n-1)\phi\cos n\phi_p$$

$$= \frac{3z}{4x_\perp}\left(\frac{2Lx_\perp}{L^2 + x_\perp^2}\right)^n\left(-2x_\perp + \frac{nL^2}{x_\perp}\right)\cos(n-1)\phi\cos n\phi_p. \tag{A4}$$

Using these simplifications, we get

$$\delta J_2 + \delta J_3 \sim \epsilon_n e^{k\alpha}\frac{(2L)^6 \gamma K p_T}{B^6}\int d\zeta dx_\perp d\phi \frac{x_\perp}{(L^2 + x_\perp^2)^3}e^U\left[4x_\perp \delta U\left(\frac{f'}{4f}U + \frac{f'}{4f} + k\right)\cos\phi\right.$$

$$\left. + 3\left(\frac{2Lx_\perp}{L^2 + x_\perp^2}\right)^n\left(U\frac{f'}{4f} + k\right)\left(-2x_\perp + \frac{nL^2}{x_\perp}\right)\cos(n-1)\phi\cos n\phi_p\right]$$

$$= \epsilon_n\frac{(2L)^6 \gamma K p_T}{B^6}\int d\zeta dx_\perp d\phi \frac{x_\perp}{(L^2 + x_\perp^2)^3}e^U\left(\frac{2Lx_\perp}{L^2 + x_\perp^2}\right)^n\left(-2x_\perp + \frac{nL^2}{x_\perp}\right)$$

$$\times \left[3z\left(\frac{f'}{4f}U + \frac{f'}{4f} + k\right)\cos\phi + 3\left(U\frac{f'}{4f} + k\right)\right]\cos(n-1)\phi\cos n\phi_p, \tag{A5}$$

where

$$U = -\frac{m_T}{T_c}\cosh(\zeta - Y) + z\cos\phi. \tag{A6}$$

Let us now define

$$Y_n(a) \equiv \int d\zeta d\phi e^{aU}\cos n\phi = 4\pi K_0(am_T/T_c)I_n(az)$$

$$\approx 4\pi K_0(am_T/T_c)\frac{1}{n!}\left(\frac{az}{2}\right)^n. \tag{A7}$$

Using this we obtain

$$\delta J_2 + \delta J_3 \approx \frac{(2L)^6 \gamma K p_T}{B^6} e^{k\alpha} \int dx_\perp \frac{x_\perp}{(L^2 + x_\perp^2)^3} \left(\frac{2Lx_\perp}{L^2 + x_\perp^2}\right)^n \left(-2x_\perp + \frac{nL^2}{x_\perp}\right)$$

$$\times \left[\frac{3z}{2}\left(\frac{f'}{4f}Y'_{n-2} + \left(\frac{f'}{4f} + k\right)Y_{n-2}\right) + 3\left(\frac{f'}{4f}Y'_{n-1} + kY_{n-1}\right)\right]_{a=1}$$

$$= 4\pi \frac{(2L)^6 \gamma K p_T}{B^6} e^{k\alpha} \int dx_\perp \frac{x_\perp}{(L^2 + x_\perp^2)^3} \left(\frac{2Lx_\perp}{L^2 + x_\perp^2}\right)^n \left(-2x_\perp + \frac{nL^2}{x_\perp}\right)$$

$$\times \frac{3n}{(n-1)!}\left(\frac{z}{2}\right)^{n-1}\left[\frac{f'}{4f}\left(-\frac{m_T}{T_c}K_1(m_T/T_c) + (n-1)K_0(m_T/T_c)\right) + kK_0(m_T/T_c)\right]$$

$$= e^{k\alpha}\frac{36\pi}{B^3}\gamma K T_c\left(\frac{64p_T}{T_c B^3}\right)^n L^3 \frac{n^2(n-1)}{3n-1}\frac{\Gamma(3n)}{\Gamma(4n)}$$

$$\times \left[\frac{f'}{4f}\left(-\frac{m_T}{T_c}K_1(m_T/T_c) + (n-1)K_0(m_T/T_c)\right) + kK_0(m_T/T_c)\right]. \tag{A8}$$

The correction to v_n can be computed analogously to (58), and the result is reported in (66).

[1] L. D. Landau and S. Z. Belenkii, On the multiparticle production in high-energy collisions, Usp. Fiz. Nauk **56**, 309 (1955).

[2] K. Adcox *et al.* (PHENIX Collaboration), Formation of dense partonic matter in relativistic nucleus-nucleus collisions at RHIC: Experimental evaluation by the PHENIX collaboration, Nucl. Phys. **A757**, 184 (2005).

[3] STAR Collaboration, Experimental and theoretical challenges in the search for the quark gluon plasma: The STAR Collaboration's critical assessment of the evidence from RHIC collisions, Nucl. Phys. **A757**, 102 (2005).

[4] B. B. Back *et al.* (PHOBOS Collaboration), The PHOBOS perspective on discoveries at RHIC, Nucl. Phys. **A757**, 28 (2005).

[5] I. Arsene *et al.* (BRAHMS Collaboration), Quark gluon plasma and color glass condensate at RHIC? The Perspective from the BRAHMS experiment, Nucl. Phys. **A757**, 1 (2005).

[6] K. Aamodt *et al.* (ALICE Collaboration), Elliptic Flow of Charged Particles in Pb-Pb Collisions at 2.76 TeV, Phys. Rev. Lett. **105**, 252302 (2010).

[7] G. Aad *et al.* (ATLAS Collaboration), Measurement of the pseudorapidity and transverse momentum dependence of the elliptic flow of charged particles in lead-lead collisions at $\sqrt{s_{NN}} = 2.76$ TeV with the ATLAS detector, Phys. Lett. B **707**, 330 (2012).

[8] CMS Collaboration, Centrality dependence of dihadron correlations and azimuthal anisotropy harmonics in PbPb collisions at $\sqrt{s_{NN}} = 2.76$ TeV, Eur. Phys. J. C **72**, 2012 (2012).

[9] J.-Y. Ollitrault, Anisotropy as a signature of transverse collective flow, Phys. Rev. D **46**, 229 (1992).

[10] A. M. Poskanzer and S. A. Voloshin, Methods for analyzing anisotropic flow in relativistic nuclear collisions, Phys. Rev. C **58**, 1671 (1998).

[11] B. Schenke, S. Jeon, and C. Gale, Elliptic and Triangular Flow in Event-by-Event $(3 + 1)$D Viscous Hydrodynamics, Phys. Rev. Lett. **106**, 042301 (2011).

[12] STAR Collaboration, Studying the phase diagram of QCD matter at RHIC, BES white paper, SN0598.

[13] STAR Collaboration, Observation of an Energy-Dependent Difference in Elliptic Flow between Particles and Antiparticles in Relativistic Heavy Ion Collisions, Phys. Rev. Lett. **110**, 142301 (2013).

[14] STAR Collaboration, Elliptic flow of identified hadrons in Au + Au collisions at $\sqrt{s_{NN}} = 7.7$–62.4 GeV, Phys. Rev. C **88**, 014902 (2013).

[15] J. D. Bjorken, Highly relativistic nucleus-nucleus collisions: The central rapidity region, Phys. Rev. D **27**, 140 (1983).

[16] S. S. Gubser, Symmetry constraints on generalizations of Bjorken flow, Phys. Rev. D **82**, 085027 (2010).

[17] S. S. Gubser and A. Yarom, Conformal hydrodynamics in Minkowski and de Sitter spacetimes, Nucl. Phys. **B846**, 469 (2011).

[18] Y. Hatta and B. W. Xiao, Building up the elliptic flow: Analytical insights, Phys. Lett. B **736**, 180 (2014).

[19] Y. Hatta, J. Noronha, G. Torrieri, and B. W. Xiao, Flow harmonics within an analytically solvable viscous hydrodynamic model, Phys. Rev. D **90**, 074026 (2014).

[20] M. Csanad, B. Tomasik, and T. Csorgo, Interplay among the azimuthally dependent HBT radii and the elliptic flow, Eur. Phys. J. A **37**, 111 (2008).

[21] R. Peschanski and E. N. Saridakis, On an exact hydrodynamic solution for the elliptic flow, Phys. Rev. C **80**, 024907 (2009).

[22] M. Csanad and A. Szabo, Multipole solution of hydrodynamics and higher order harmonics, Phys. Rev. C **90**, 054911 (2014).

[23] P. F. Kolb, J. Sollfrank, and U. W. Heinz, Anisotropic transverse flow and the quark hadron phase transition, Phys. Rev. C **62**, 054909 (2000).

[24] D. Teaney, J. Lauret, and E. V. Shuryak, A hydrodynamic description of heavy ion collisions at the SPS and RHIC, arXiv:nucl-th/0110037.

[25] H. Petersen and M. Bleicher, Ideal hydrodynamics and elliptic flow at SPS energies: Importance of the initial conditions, Phys. Rev. C **79,** 054904 (2009).

[26] C. Shen and U. Heinz, Collision energy dependence of viscous hydrodynamic flow in relativistic heavy-ion collisions, Phys. Rev. C **85,** 054902 (2012); **86,** 049903(E) (2012).

[27] I. A. Karpenko, P. Huovinen, H. Petersen, and M. Bleicher, Estimation of the shear viscosity at finite net-baryon density from A + A collision data at $\sqrt{s_{NN}}$ = 7.7–200 GeV, Phys. Rev. C **91,** 064901 (2015).

[28] C. Alt *et al.* (NA49 Collaboration), Directed and elliptic flow of charged pions and protons in Pb + Pb collisions at 40-A-GeV and 158-A-GeV, Phys. Rev. C **68,** 034903 (2003).

[29] CMS Collaboration, Studies of azimuthal dihadron correlations in ultracentral PbPb collisions at $\sqrt{s_{NN}}$ = 2.76 TeV, J. High Energy Phys. 02 (2014) 088.

[30] F. Cooper and G. Frye, Comment on the single particle distribution in the hydrodynamic and statistical thermodynamic models of multiparticle production, Phys. Rev. D **10,** 186 (1974).

[31] K. Dusling, G. D. Moore, and D. Teaney, Radiative energy loss and v(2) spectra for viscous hydrodynamics, Phys. Rev. C **81,** 034907 (2010).

[32] P. Staig and E. Shuryak, The fate of the initial state fluctuations in heavy ion collisions. III The second act of hydrodynamics, Phys. Rev. C **84,** 044912 (2011).

[33] J. Erdmenger, M. Haack, M. Kaminski, and A. Yarom, Fluid dynamics of R-charged black holes, J. High Energy Phys. 01 (2009) 055.

[34] J. Cleymans, H. Oeschler, K. Redlich, and S. Wheaton, Comparison of chemical freeze-out criteria in heavy-ion collisions, Phys. Rev. C **73,** 034905 (2006).

[35] A. Andronic and P. Braun-Munzinger, Ultrarelativistic nucleus-nucleus collisions and the quark gluon plasma, Lect. Notes Phys. **652,** 35 (2004).

[36] A. Andronic, An overview of the experimental study of quark-gluon matter in high-energy nucleus-nucleus collisions, Int. J. Mod. Phys. A **29,** 1430047 (2014).

[37] CMS Collaboration, Azimuthal anisotropy harmonics in ultracentral PbPb collisions at $\sqrt{s_{NN}}$ = 2.76 TeV, Report No. CMS-PAS-HIN-12-011.

[38] STAR Collaboration, Beam energy dependence of first and higher order flow harmonics from the STAR experiment at RHIC, Nucl. Phys. **A904–A905,** 357c (2013).

[39] STAR Collaboration, Inclusive charged hadron elliptic flow in Au + Au collisions at $\sqrt{s_{NN}}$ = 7.7–39 GeV, Phys. Rev. C **86,** 054908 (2012).

[40] S. Esumi (PHENIX Collaboration), Identified charged particle azimuthal anisotropy in PHENIX at RHIC, Nucl. Phys. **A715,** 599c (2003).

[41] STAR Collaboration, Correlations, fluctuations, and flow measurements from the STAR experiment, Nucl. Phys. **A715,** 45c (2003).

[42] Y. Burnier, D. E. Kharzeev, J. Liao, and H. U. Yee, Chiral Magnetic Wave at Finite Baryon Density and the Electric Quadrupole Moment of Quark-Gluon Plasma in Heavy Ion Collisions, Phys. Rev. Lett. **107,** 052303 (2011).

[43] J. Steinheimer, V. Koch, and M. Bleicher, Hydrodynamics at large baryon densities: Understanding proton versus antiproton v_2 and other puzzles, Phys. Rev. C **86,** 044903 (2012).

[44] J. Xu, T. Song, C. M. Ko, and F. Li, Elliptic Flow Splitting as a Probe of the QCD Phase Structure at Finite Baryon Chemical Potential, Phys. Rev. Lett. **112,** 012301 (2014).

[45] M. Hongo, Y. Hirono, and T. Hirano, First numerical simulations of anomalous hydrodynamics, arXiv:1309.2823.

[46] P. Braun-Munzinger, I. Heppe, and J. Stachel, Chemical equilibration in Pb + Pb collisions at the SPS, Phys. Lett. B **465,** 15 (1999).

[47] STAR Collaboration, Beam energy dependence of strange hadron production from STAR at RHIC, J. Phys. Conf. Ser. **509,** 012085 (2014).

[48] A. Bazavov, H. T. Ding, P. Hegde, O. Kaczmarek, F. Karsch, E. Laermann, S. Mukherjee, P. Petreczky *et al.*, Freeze-out Conditions in Heavy Ion Collisions from QCD Thermodynamics, Phys. Rev. Lett. **109,** 192302 (2012).

[49] A. Bazavov, H.-T. Ding, P. Hegde, O. Kaczmarek, F. Karsch, E. Laermann, Y. Maezawa, S. Mukherjee *et al.*, Additional Strange Hadrons from QCD Thermodynamics and Strangeness Freezeout in Heavy Ion Collisions, Phys. Rev. Lett. **113,** 072001 (2014).

[50] A. Andronic (private communication).

[51] S. A. Voloshin, Anisotropic flow from AGS to RHIC, arXiv: nucl-th/0202072.